

See discussions, stats, and author profiles for this publication at: <https://www.researchgate.net/publication/274375980>

Redox Active Polyaniline-h-MoO₃ Hollow Nanorods for Improved Pseudocapacitive Performance

ARTICLE *in* THE JOURNAL OF PHYSICAL CHEMISTRY C · MARCH 2015

Impact Factor: 4.77 · DOI: 10.1021/acs.jpcc.5b00153

CITATIONS

3

READS

129

2 AUTHORS, INCLUDING:



Vipin Kumar

Nanyang Technological University

19 PUBLICATIONS 36 CITATIONS

[SEE PROFILE](#)

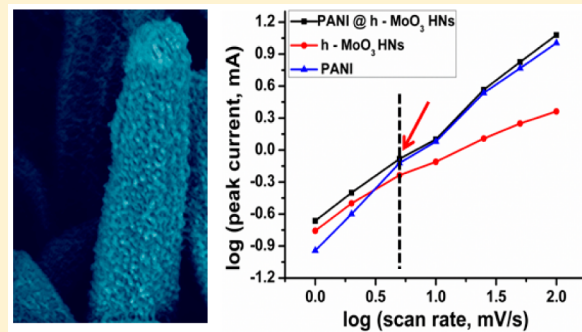
Redox Active Polyaniline-h-MoO₃ Hollow Nanorods for Improved Pseudocapacitive Performance

Vipin Kumar and Pooi See Lee*

School of Materials Science and Engineering, Nanyang Technological University, 50 Nanyang Avenue, Singapore 639798, Singapore

S Supporting Information

ABSTRACT: Combinatorial approaches in preparing nanocomposites of transition metal oxides with conductive polymers have gained enormous attention due to their outstanding pseudocapacitive properties which are mainly associated with the solid-state diffusion of electrolyte ions as well as surface or near-surface reversible redox reactions. Here, we elaborate on the interplay of surface-controlled and diffusion-controlled redox reactions based on polyaniline and hexagonal molybdenum trioxide (h-MoO₃) hollow nanorods to realize improved electrochemical performance of the nanocomposite electrode. The cationic species (Ferric ions) were used as the oxidants to polymerize aniline monomers and assist in the formation of h-MoO₃ hollow nanorods. The formation of h-MoO₃ hollow nanorods was realized through the cation exchange-assisted Kirkendall effect driven by ferric ions. The resultant core–shell architecture of the polymerized h-MoO₃ showed improved pseudocapacitive performance (270 F/g) when compared to the pristine h-MoO₃ hollow nanorods (126 F/g) or polyaniline (180 F/g) at a current density of 1 A/g, with enhanced cycling stability.



1. INTRODUCTION

Due to an increasing demand of portable and high-performance electronic devices, electrochemical capacitors or supercapacitors are considered as a promising candidate due to their fast charging/discharging rate, excellent rate capability, and ultra-long cycling stability.¹ Supercapacitors are the alternative charge-storage devices, which fill the gap between conventional capacitors and batteries in terms of the energy density and power density.^{1–4} Supercapacitors can be classified into two main categories based on their charge-storage mechanism, i.e., electric double-layer capacitor and pseudocapacitor.⁵ In the electric double-layer capacitor (EDLC), separation of the electronic and ionic charges takes place at the interface, developed between high surface area electrode materials (such as carbon or carbon-based materials) and electrolyte.⁶ On the other hand, pseudocapacitors involve the fast faradic redox reactions associated with the solid-state diffusion of electrolyte ions (intercalation pseudocapacitance),⁷ as well as surface or near-surface redox reactions (surface pseudocapacitance).⁸ MnO₂, RuO₂·xH₂O, T-Nb₂O₅, polyaniline, etc.^{9–12} are the ideal candidates to show intercalation and surface pseudocapacitance. The principal benefit realized from pseudocapacitive materials is that the high level of charge storage can be achieved in a short period of time contributed from the fast redox reactions, i.e., surface or near-surface and solid-state diffusion.

Among the transition metal oxides, nanostructures of molybdenum trioxide have become a subject of increasing interest due to the high electrochemical activity (availability of multiple oxidation states) of its stable and metastable

polymorphs (α -MoO₃, β -MoO₃, h-MoO₃, MoO₃-II, etc.) and eco-friendly nature.^{13,14} MoO₃ polymorphs exist in the form of crystalline hydrates; for example, dihydrated MoO₃ (MoO₃·2H₂O) is found to be monoclinic ($P2_1/n$), and monohydrated MoO₃ (MoO₃·H₂O) exists in triclinic ($P-1$) (white appearance) and monoclinic ($P2_1/c$) (yellow appearance). Moreover, hemihydrated MoO₃ (MoO₃·0.5H₂O) exists as monoclinic ($P2_1/m$) as well as orthorhombic (C^*/\ast).^{15,16} It is worth mentioning that all the hydrated forms of MoO₃, i.e., MoO₃·2H₂O, MoO₃·H₂O, and MoO₃·0.5H₂O, transform to the stable phase of MoO₃, i.e., α -MoO₃ phase on the application of temperature (350–400 °C).¹⁶ Apart from such spectacular features, it has showed its potential to be used in a variety of fields, such as light-emitting diodes, platform for tunable plasmon resonance,¹⁷ organic solar cell device,¹⁸ FET-based chemical, biological as well as multiple gas sensors,^{19–22} and a lubricant in the large-scale industries.²³ MoO₃ is an excellent example of prospective electrode materials for batteries with high theoretical capacity (1117 mA h/g), and it has been demonstrated as both cathode and anode materials.^{24–26} MoO₃ has also been used in electrochemical capacitors as a pseudocapacitive (intercalation pseudocapacitance) electrode material due to its high theoretical specific capacitance (~2700 F/g) and fast faradic redox reaction kinetics.^{7,27} In practice, the poor electronic conductivity of MoO₃ prohibits it from

Received: January 6, 2015

Revised: March 30, 2015



ACS Publications

© XXXX American Chemical Society

A

DOI: 10.1021/acs.jpcc.5b00153
J. Phys. Chem. C XXXX, XXX, XXX–XXX

achieving theoretical performance even in its nanostructured form. Extensive research efforts have been exerted to improve reaction kinetics and cycling stability by tuning the shape and size; however, the improvements have not been significant.^{28,29} Most recently, it is demonstrated that the electrochemical performance of MoO₃ nanostructures can be improved with the open structure of MoO₃, i.e., hexagonal phase of MoO₃ (h-MoO₃) and graphene nanocomposites.³⁰ To overcome these shortcomings associated with MoO₃ nanostructures, several strategies were adopted. Among them, coating of conductive supports, such as conductive polymers (due to their tunable physical-chemical properties), has been adopted in the recent years. Most recently, Hu et al.³¹ proposed coaxial structure of polyaniline/MoO₃ nanobelts to address poor electrochemical activity of MoO₃, but tens of percentage degradation within few hundreds of cycles could not meet with the requirements. Moreover, Wu et al.³² and Qi et al.³³ also adopted a coaxial nanowires strategy using polypyrrole as the conductive support to improve electrochemical performance of the nanocomposite, i.e., polypyrrole/MoO₃ nanorods, but lack of prolonged cycling stability data could not conclude actual improvement in the electrochemical performance. Therefore, to resolve the pitiable electrochemical performance of the nanocomposites, we propose a combinatory approach of modifying not only the surface of the nanorods but also physical structure (in transforming solid nanorods into hollow nanorods) to minimize the boundaries between electrode and electrolyte.

The physical structure of the materials can be altered using self-template methods such as Kirkendall effect,³⁴ Galvanic replacement,³⁵ cationic or anionic replacement,³⁶ and Ostwald ripening.³⁷ These strategies are advantageous to produce hollow micro/nanostructures with controllable pore structures and compositions, which are essential to promote the electrochemical reactions.³⁸ Hollow micro/nanostructured materials have been recognized as one of the promising features in energy-related applications. The unique physical structure of hollow nanostructures provides higher active surface area, short diffusion path for electrolyte ions, improved cycling life (it can accommodate a large volume change during charge/discharge), and effective utilization of the active materials.³⁹ Attributed to the spectacular features associated with the hollow nanostructures, they can be used in various applications; for example, hollow spheres of metal or metal oxides have been used as photoanodes,⁴⁰ support materials in fuel cells,⁴¹ a high-performance capacitor,⁴² and high-performance electrode materials in lithium ion batteries and supercapacitors.^{43,44} In the past several years, only single-shell materials have been reported. However, there have been little efforts on complex-hollow structures with multiple shells that can be considered to further tune the properties of hollow micro/nanostructured materials. Recently, Wu et al.⁴⁵ and Yuan et al.⁴⁶ have demonstrated the use of hollow nanocomposites using graphene/MnO₂ and graphene/Co₃S₄ hollow nanospheres, respectively, to realize improved electrochemical performance. On the other hand, Fan et al.⁴⁷ illustrated that the gap between the constituents is essential to grasp an improved electrochemical performance. In their demonstration, they used TiO₂ nanotubes to enclose NiO or CoO nanowalls, forming “wall in box” geometry. Most recently, Liu et al.⁴⁸ used hollow CuO@MnO₂ nanostructures to improve cycling stability of the hybrid electrode up to 93% of its initial value upon 1000 cycles. In this work, we design and synthesize the

hollow hybrid nanocomposites and address the mechanism of charge storage in this type of complex hybrid system.

In the present study, we describe the formation of h-MoO₃ hollow nanorods (hereafter named h-MoO₃ HNs) using the cation-exchange-assisted Kirkendall effect. A facile chemical polymerization of the as-prepared hollow nanorods is demonstrated using aniline monomers as the basic unit. The fast and efficient oxidative chemical polymerization of aniline is realized due to the unique surface chemistry of h-MoO₃ HNs. Attributed to the surface-controlled and diffusion-controlled redox reactions (associated with polyaniline (PANI) and h-MoO₃), an improved specific capacitance and cycling stability of PANI@h-MoO₃ HNs is accomplished.

2. EXPERIMENTAL SECTION

2.1. Chemical Used. Molybdenum powder (99.9%), hexamethylenetetramine (HMTA), hydrogen peroxide (H₂O₂-30%), aniline (C₆H₅NH₂), ferric chloride hexahydrate (FeCl₃·6H₂O), and hydrochloric acid (HCl) were purchased from Alfa Aesar and Sigma-Aldrich.

2.2. Synthesis of h-MoO₃ Nanorods. All the chemical reagents were used as purchased without further purification. The synthesis of h-MoO₃ nanorods is described in our previous reports.⁴⁹ Briefly, a solution of 100 mg of HMTA was prepared in 10 mL of DI water and mixed into a 20 mL glass vial containing 5 mL of peroxomolybdic acid solution. The as-obtained yellow solution was left for stirring for several hours (~8 h) and kept in a lab oven for 18 h at 100 °C. The precipitate was collected by centrifugation, washed in ethanol and DI water, and then dried at 80 °C for overnight.

2.3. Preparation of h-MoO₃ Hollow Nanorods (h-MoO₃ HNs). In order to realize the formation of h-MoO₃ hollow nanorod structure, a cation-exchange-assisted Kirkendall effect approach was employed.⁵⁰ In this typical synthesis procedure, 100 mg of h-MoO₃ nanorods was dispersed in 0.36 M FeCl₃·6H₂O solution and left under stirring for 20 min at room temperature. An aging of 24 h was then performed to obtain h-MoO₃ HN powder.

2.4. Synthesis of Polyaniline@h-MoO₃ Hollow Nano-rods (PANI@h-MoO₃ HNs). In this typical synthesis procedure, 100 mg of the as-synthesized h-MoO₃ nanorods was dispersed into 0.36 M FeCl₃·6H₂O solution under vigorous magnetic stirring and left for 20 min at room temperature. The anilinium chloride solution was prepared by mixing 100 μL, 150 μL, and 200 μL of aniline into 2.6 M HCl. To decorate PANI on h-MoO₃ nanorods, the molar ratio of oxidant (FeCl₃·6H₂O) to aniline monomers was varied from ~1 to ~1.2 to 1.7. The as-prepared anilinium salt solution was dropwise added into the nanorod solution under magnetic stirring at a constant temperature of 60 °C. The color of the solution gradually changed from khaki to deep green on mixing of anilinium chloride solution, which confirms the commencement of polymerization, and this reaction was continued for 3 h. After aging at room temperature for 24 h, the precipitate was collected by centrifugation, washed with ethanol and DI water, and then dried at 80 °C overnight. Among the various nanocomposites of PANI@h-MoO₃ HNs, the nanocomposites prepared using molar ratio (oxidant/aniline) ~ 1 were chosen for further characterizations.

2.4. Electrode Preparation for Electrochemical Testing. The working electrode was prepared by mixing of the as-prepared samples (h-MoO₃ HNs, polyaniline, and PANI@h-MoO₃ HNs) powder (85%), carbon black (10%), and PVDF

(5%) into a 5 mL vial containing 500 μ L of NMP. An amount of 20 μ L of this slurry was coated onto a current collector (graphite paper, 1 cm^2) and dried in a laboratory oven at 100 $^\circ\text{C}$. The loading mass of active material was measured to be 1 \pm 0.05 mg for all three samples. Electrochemical testing was done in an aqueous solution of H_2SO_4 (1 M) in a potential window of 0–0.65 V vs Ag/AgCl.

2.5. Characterizations of the Materials. The samples were characterized using powder X-ray diffractometry (Shimadzu XRD – 6000, Cu K α radiation $\lambda = 1.54 \text{ \AA}$; power, 2 kW) at a scan rate of 1°/min in the 2 theta range of 10°–60°. Field emission scanning electron microscopy (FESEM; JEOL, JSM 7600F thermal FEG, JSM 6340F cold cathode FEG) and transmission electron microscopy (TEM; JEOL, JEM 2010 and JEM 2100F) were used to evaluate the morphology of the samples. Thermal analyses were done using differential scanning calorimetry (DSC)/differential thermal analysis (DTA) (STA-449 C, max temperature 1500 $^\circ\text{C}$) and thermogravimetric analysis (TGA) (Q 500, Max. Temperature 900 $^\circ\text{C}$). IR spectroscopy (PerkinElmer, Model Spectrum GX) was used to extract the information about the functional groups present in pristine h-MoO₃ HNs as well as polyaniline decorated h-MoO₃ HNs. Electrochemical measurements were carried out using Solartron, S1470E electrochemical interface. A three-electrode cell configuration was used for electrochemical testing, in which active materials (h-MoO₃ HNs, PANI, and PANI@h-MoO₃ HNs) coated graphite paper (1 cm^2), platinum sheet, and saturated Ag/AgCl electrode were employed as working, counter, and reference electrode, respectively, in an aqueous electrolyte (1 M H_2SO_4). Electrochemical impedance spectroscopy (EIS) measurements were carried out by applying an AC voltage with 1 mV amplitude in a frequency range from 100 kHz to 100 mHz at open-circuit potential (OCP).

3. RESULTS AND DISCUSSION

The crystallographic structure or phase of the as-prepared nanocomposites was investigated using XRD. Figure 1 shows

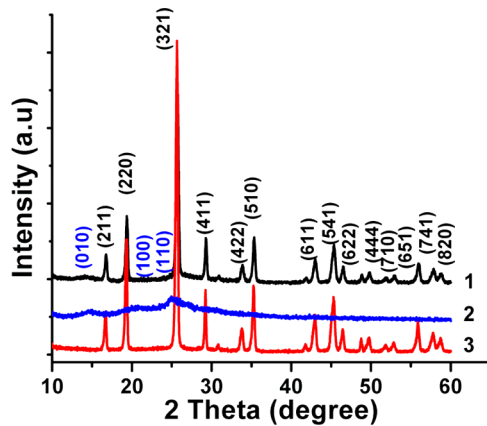


Figure 1. XRD patterns of (1) PANI@h-MoO₃ HNs, (2) PANI, and (3) h-MoO₃ HNs.

X-ray diffraction patterns of the as-prepared PANI@h-MoO₃ HNs, PANI, and h-MoO₃ HNs. The XRD patterns of h-MoO₃ HNs and PANI@h-MoO₃ HNs can be indexed according to the hexagonal phase of MoO₃ (ICDD card 29-0115). A peak at $2\theta \sim 14.4$ in the spectra of PANI indicates the signature of the monoclinic phase of PANI,⁵¹ while peaks at $2\theta \sim 20.4$ and $2\theta \sim 25.2$ in the spectra of PANI show the periodicity of the

partially reduced and oxidized chains is parallel and perpendicular to aniline chains. This peak also represents the distance between two adjacent benzene rings.⁵² An intense peak in the spectra of PANI@h-MoO₃ HNs and h-MoO₃ HNs at $2\theta \sim 25.6$ depicts the hexagonal phase of MoO₃ as well as the coexistence of PANI at h-MoO₃ HNs. The peak position in the diffraction spectra of PANI@h-MoO₃ HNs was found unchanged, as it was in h-MoO₃ HNs, which indicates that polymerization of the aniline monomers strictly happens on the surface of the nanorods.

The formation of hexagonal MoO₃ (h-MoO₃ phase) may sometimes resemble hydrated polymorphs of MoO₃.⁵³ It has to be noted that H₂O molecules in hydrated MoO₃ are loosely attached with the MoO₆ octahedra and accountable to accelerate the phase transformation even at moderate temperature, e.g., 350 $^\circ\text{C}$.¹⁶ In the hydrated form of MoO₃, most of the weight loss occurs due to removal of H₂O molecules. On the other hand, H₂O molecules in hexagonal structure are not only attached with MoO₆ octahedra but also confined in the local field of the structure-stabilizing ions, e.g., NH₄⁺ ions.^{53,54} The hexagonal structure remains stable as long as the stabilizing ions are present in the structure. In general, structure-stabilizing ions leave the structure at about 500 $^\circ\text{C}$, as discussed in our previous report.⁵⁵ Therefore, the stability of the structure and phase transformation temperature of the hexagonal phase of MoO₃ distinguishes it from the hydrated form of MoO₃. DSC and XRD analyses of the sample after thermal treatments are presented in the Supporting Information, Figure S1. DSC analysis (Figure S1(a)) shows that the phase transformation is limited by the structure-stabilizing ions, i.e., NH₄⁺ and phase of the material changes after extraction of NH₄⁺ ions at about 450 $^\circ\text{C}$. XRD results show that the phase of the material remains unchanged even after annealing at 400 $^\circ\text{C}$, as shown in Figure S1(b).

The morphology and physical structure of h-MoO₃ HNs and PANI@h-MoO₃ HNs were investigated using FESEM and TEM, as shown in Figure 2. The pyramidal hollow nanorod-like morphology can be seen in Figure 2(a). Figure 2(b) indicates the morphology of the hollow nanorods after polymerization. FESEM micrograph of h-MoO₃ nanorods and pure PANI are shown in the Supporting Information, Figure S2. From TEM micrographs, it is evident that the as-polymerized nanorods form a core–shell structure, as can be seen clearly in Figure 2(d). Figure 2(c) shows TEM micrograph of the pristine h-MoO₃ HNs. The thickness and morphology of the PANI shell at the surface of h-MoO₃ HNs were controlled by the molar ratio of oxidant to aniline, i.e., 1.2 and 1.7. With an increasing molar ratio of oxidant to aniline, the PANI coating changes from fractal-like shell to a more uniform and smooth layer as evaluated by TEM analysis (shown in Supporting Information, Figure S3).

The presence of a PANI shell at h-MoO₃ HNs was further evaluated by IR spectroscopy in absorption mode, as shown in Figure 3. The absorption peaks at 692, 868, and 966 cm^{-1} were observed in the spectra of pristine h-MoO₃ HNs and PANI@h-MoO₃ HNs, which can be assigned to an in-plane vibration of MoO₄²⁻ units, stretching of the O–O bond, and stretching of the terminal oxygen (M=O) atom, respectively (IR spectrum of h-MoO₃ nanorods is shown in Supporting Information, Figure S3). The bands at 1428 cm^{-1} and at 1609 cm^{-1} are attributed to the stretching and deformation of NH₄⁺ and absorbed –OH groups on the surface of h-MoO₃, respectively.⁴⁹ Interestingly, the intensity of the band at 868 cm^{-1}

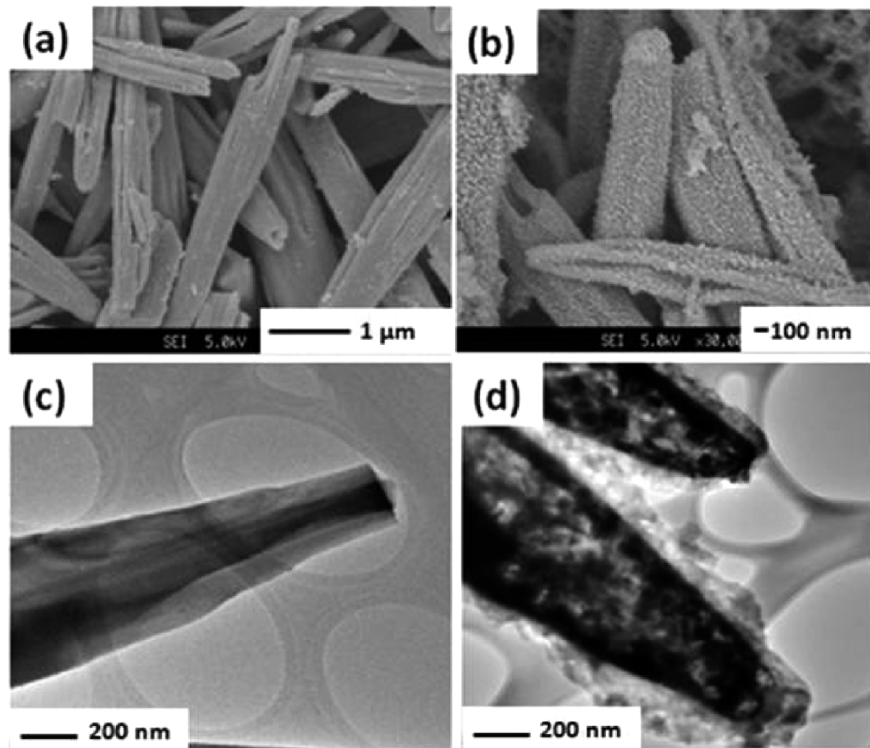


Figure 2. FESEM micrographs of (a) h-MoO₃ HNs and (b) PANI@h-MoO₃ HNs and TEM micrographs of (c) h-MoO₃ HNs and (d) PANI@h-MoO₃ HNs.

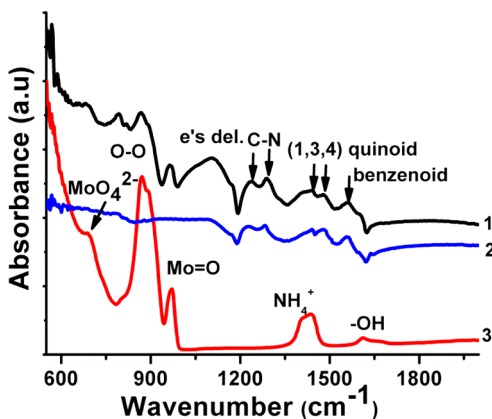


Figure 3. IR spectra of (1) PANI@h-MoO₃ HNs, (2) PANI, and (3) h-MoO₃ HNs.

decreased significantly after the polymerization at the surface of h-MoO₃ HNs. This suggests that the protonated nitrogen atoms of anilinium salt prefer to attach with the surface oxygen atoms, while the absence of the band at 1609 cm⁻¹ in the case of PANI@h-MoO₃ HNs depicts the consumption of -OH groups during the attachment process. An IR band at 1107 cm⁻¹ indicates delocalization of electrons in PANI and stretching of N=Q=N (Q is quinoid ring). A couple of bands that appear at 1233 and 1291 cm⁻¹ can be assigned to the stretching of the C-N bond. The vibration of rings 1, 3, and 4 in the chain of PANI is observed at 1441 cm⁻¹. The IR bands corresponding to stretching vibration of the quinoid and benzenoid ring are observed at 1479 and 1564 cm⁻¹, respectively, suggesting the as-prepared PANI is in an emeraldine state rather than a leucoemeraldine or pernigraniline state.^{56,57} Therefore, IR spectroscopy confirms the

existence of both the constituents, i.e., PANI and h-MoO₃, in the as-prepared nanocomposites of PANI@h-MoO₃ HNs. Moreover, TGA confirms the existence of PANI in the PANI@h-MoO₃ HN nanocomposites, as shown in the Supporting Information, Figure S5. IR spectra of PANI@h-MoO₃ HNs (prepared using a higher molar ratio of oxidant to aniline, i.e., 1.7 and 1.2) depict that as the molar ratio increases a blue shift in the IR band (corresponding to delocalization) was observed, as shown in the Supporting Information, Figure S4. This shift in the band may be ascribed to the overoxidation of PANI chains due to the relatively high concentration of the oxidant ions.⁵⁸

3.1. Formation of h-MoO₃ HNs and Mechanism of Their Polymerization. The oxidative chemical polymerization of anilinium chloride salt (protonated form of aniline in hydrochloric acid) monomers is widely accepted.⁵⁹ The formation of hollow nanorod structures of h-MoO₃ and their polymerization mechanism can be described on the basis of the mechanism illustrated in Figure 4.

MoO₃ is an acidic transition metal oxide, and the pH value of nanorod solution in our case was found to be ~4.3 at room



Figure 4. Schematic representation of the steps involved during the formation of h-MoO₃ hollow nanorods and their oxidative chemical polymerization of aniline using ferric ions.

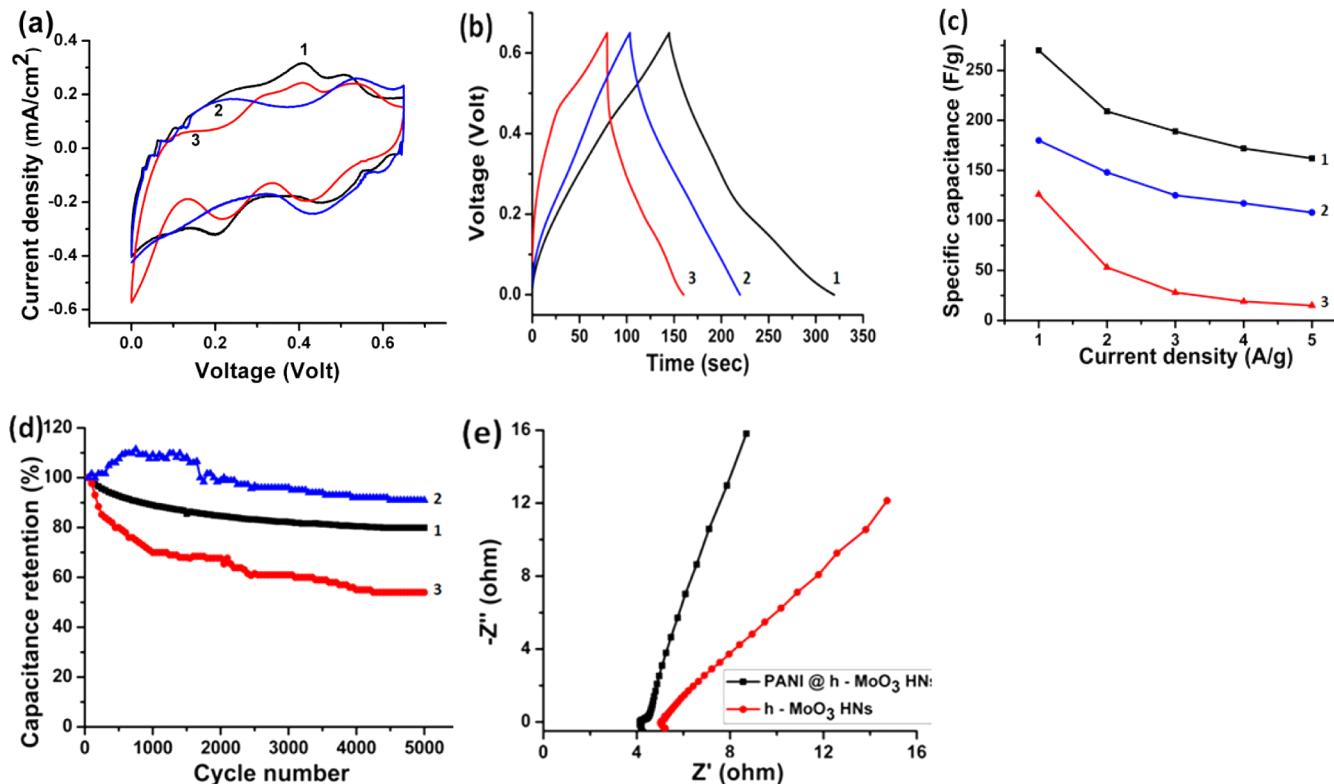


Figure 5. Cyclic voltammograms of (1) PANI@h-MoO₃ HNs, (2) PANI, and (3) h-MoO₃ HNs at a scan rates of (a) 1 mV/s, (b) charge–discharge curves of all three types of samples at an applied current density of 1 A/g, (c) specific capacitance as a function of applied current density for all three types of samples, (d) cycling stability of the electrodes at a scan rate of 50 mV/s, and (e) Nyquist plot of PANI@h-MoO₃ HNs and h-MoO₃ HNs in the frequency range of 100 kHz to 100 mHz.

temperature. When a solution of Fe³⁺ ions reacts with h-MoO₃ nanorods, the formation of h-MoO₃ HNs was realized, which can be explained on the basis of the cation-exchange-assisted Kirkendall effect.^{22,50,60} The exchange of a cation takes place in a polar solvent containing the solvated form of ionic salt and a nonsolvated form of ionic or polar compounds. Here, we used water as a solvent containing the solvated form of Fe³⁺ ions and the nonsolvated form of h-MoO₃ nanorods. This ion exchange mechanism is assisted by the exchange of Mo⁶⁺ cations with the Fe³⁺ ions due to the availability of the negatively charged functional groups (−OH) at the surface. The cation exchange mechanism can be explained as follows: (1) movement of Fe³⁺ ions near to the surface layer and inward diffusion of ions through the pores of the h-MoO₃, (2) exchange of Mo⁶⁺ cations with Fe³⁺ ions, (3) outward diffusion of exchanged Mo⁶⁺ ions through the pores of h-MoO₃, and (4) movement of the exchanged Mo⁶⁺ ions into the bulk solution. The rate of this reaction is controlled by the diffusion of Fe³⁺ ions into the bulk h-MoO₃. Therefore, bulk h-MoO₃ dissolves into the ionic solution via removal of Mo⁶⁺ ions and only anionic structure intact with the parent framework, which is accountable to form a hollow network.⁶¹ The anilinium monomers (conjugated acid of aniline) have pK_a value of the order of ~4.6, with a positively charged nitrogen atom.⁵⁸ Simultaneously, oxidation and attachment of monomer units happened on the surface of h-MoO₃ attributed to the Fe³⁺ ions and the presence of −OH functional groups, respectively. The attachment of the polyaniline unit with the surface of h-MoO₃ HNs (PANI@h-MoO₃ HNs) is the result of having high density of hydroxyl groups and unsaturated oxygen ions as evaluated by IR spectroscopy.

3.2. Electrochemical Properties of PANI @ h-MoO₃ HNs.

The obvious benefit of using hollow nanostructures is that they increase the number of accessible active sites, significantly reducing the diffusion path for the ions, and they can accommodate a large volume change, which is essential to realize an improved cycling life. It is evident from the CV analysis that the h-MoO₃ HNs have better charge storage capability (wider area under CV curve) than that of their bulk counterpart, i.e., nanorods, as presented in the Supporting Information, Figure S6. The electrochemical performances of PANI@h-MoO₃ HNs, PANI, and h-MoO₃ HNs were investigated using cyclic voltammograms (CVs) and galvanic charge–discharge methods. As shown in Figure 5(a), the presence of PANI further improves the charge storage capacity of h-MoO₃ HNs. The presence of redox peaks in CV indicates that the process involves faradic redox reactions. At a slow scan rate (1 mV/s), significant redox peaks appeared at 0.40 V/0.23 and 0.49 V/0.44 V [corresponding to different intercalation (Mo⁶⁺ > Mo⁵⁺) sites] in h-MoO₃. For PANI, redox peaks appeared at 0.22 V/0.12 V and 0.53 V/0.43 V, corresponding to the transition from semiconducting state (leuco emeraldine form) to conducting state (polaronic emeraldine form) and faradic transformation of emeraldine to pernigraniline state, respectively. Nanocomposites of PANI@h-MoO₃ HNs show the characteristics of both the constituents, i.e., h-MoO₃ and PANI, as shown in Figure 5(a).

In contrast, when the scan rate is sufficiently high (100 mV/s), only those ions immediately next to the interface respond to the external field, which results in increased capacitive behavior (associated with the fast surface redox reactions) of the electrode, as shown in the Supporting Information, Figure S7.

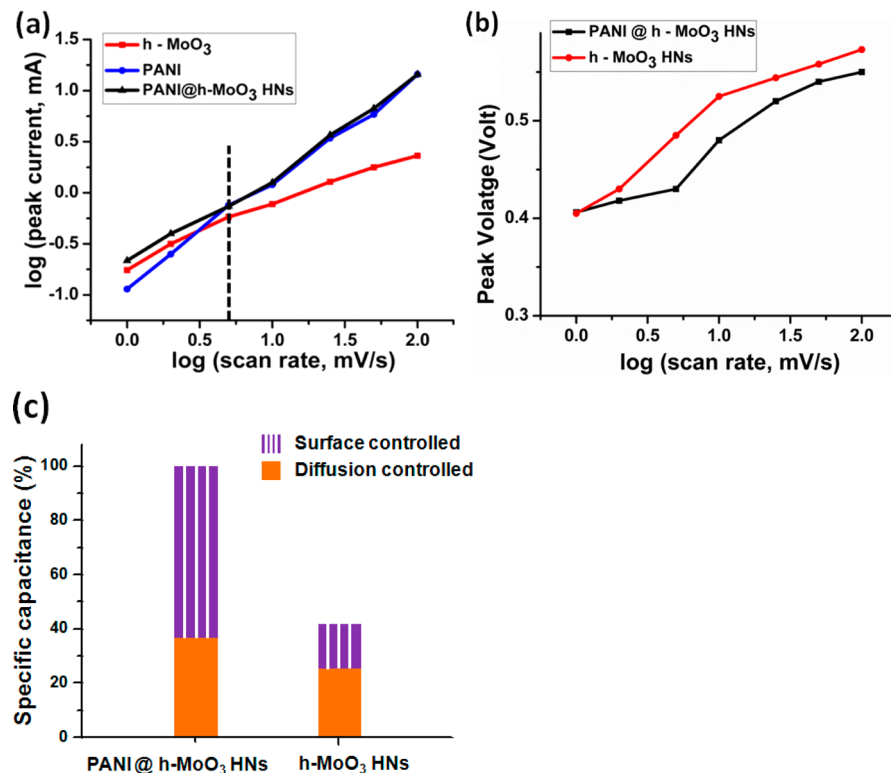


Figure 6. (a) Cathodic peak current as a function of scan rate, (b) cathodic peak voltage as a function of scan rates, and (c) the contribution of surface- and diffusion-controlled charge transfer kinetics in h-MoO₃ HNs and PANI@h-MoO₃ HNs.

This indicates PANI plays a vital role to enhance the charge-storage capability of the nanocomposites. CVs of all three types of samples at higher scan rates are presented in the Supporting Information, Figure S7. The nanocomposites prepared using an oxidant/aniline molar ratio ~ 1 are found to be better than that of the rest of the nanocomposites prepared using higher molar ratios, as shown in the cyclic voltammograms (Supporting Information, Figure S8).

The specific capacitance is measured using galvanic charge–discharge method. Charge–discharge curves and specific capacitance as a function of current density for all three types of samples are shown in Figure 5(b) and (c), respectively. PANI@h-MoO₃ HNs show high specific capacitance of 270 F/g at an applied current density of 1 A/g, while it maintains 162 F/g at 5 A/g. This shows an improved rate capability when compared with h-MoO₃ HNs. The specific capacitance of PANI@h-MoO₃ HNs was found to be higher than PANI/ α -MoO₃ nanoparticles (200 F/g),⁶² PANI/ α -MoO₃ nanotubes, and nanosheets (180 and 200 F/g),⁶³ and polypyrrole/ α -MoO₃ nanorods (110 and 129 F/g).^{32,33} A study on PANI/ α -MoO₃ nanobelts showed a high specific capacitance value of 632 F/g; however, the loading mass is low (~ 0.01 mg), and the mechanism has not been elucidated.³¹ The improved specific capacitance of PANI@h-MoO₃ HNs suggests the merit of PANI in the nanocomposites by creating a fast electron conduction path. The charge–discharge curves of all three types of samples at various applied current densities are shown in the Supporting Information, Figure S9. Galvanic charge–discharge curves of the nanocomposites prepared using higher oxidant to aniline molar ratios are shown in the Supporting Information, Figure S10.

The presence of PANI also improves the cycling stability of the nanocomposites by prompting rate of redox reactions and

retaining $\sim 80\%$ of the initial capacitance upon 5000 charge–discharge cycles of CV, as shown in Figure 5(d). On the other hand, early stage improvement and degradation in the stability of PANI and MoO₃ are associated with the activation of polymer chains and breakage of nanorods, respectively.^{63,64} The stability of PANI@h-MoO₃ HNs was found to be better than that of the PANI/ α -MoO₃ nanobelts (76% after 3000 cycles)³¹ and polypyrrole/ α -MoO₃ nanorods ($\sim 80\%$ after 600 cycles).³² This improvement in the cycling stability of the nanocomposite of PANI@h-MoO₃ HNs can be credited to the hollow structure of the nanorods (hollow structures can accommodate higher strain produced during charge–discharge) and the existence of the PANI shell (which not only anchored h-MoO₃ HNs but also provide an effective highway for the transportation of the charges). Therefore, The combinatory approach of hollow hybrid nanocomposites is beneficial to realize improved cycling stability.

The electrode–electrolyte resistance and charge transfer resistance of the as-prepared electrodes in the frequency range of 100 kHz to 100 mHz were studied using electrochemical impedance spectroscopy (EIS). The Nyquist plots of h-MoO₃ HNs and PANI@h-MoO₃ are shown in Figure 5(e). The Nyquist plot shows the relationship between the real and imaginary component of the impedance offered by the electrode/electrolyte system. The Nyquist plot can be divided into two regions: the high frequency semicircle region—indicates solution resistance, contact resistance, and charge transfer resistance—and a low frequency straight line region—indicates diffusion resistance (Warburg element).⁶⁵ PANI@h-MoO₃ HNs show low solution as well as charge transfer resistance for faradic reactions in comparison with the pristine h-MoO₃ HNs. A quasicapacitive and purely resistive (Warburg element) behavior was observed in PANI@h-MoO₃ HNs and

h-MoO₃ HNs electrodes, respectively. The reduced charge transfer resistance of PANI@h-MoO₃ HNs results in better rate capability because it acts as a limiting factor in faradic reactions.⁶⁶

The mechanism of this enhancement in electrochemical performance of PANI@h-MoO₃ can be deconvoluted by considering that the current obeys the power-law relationship with the scan rate, which leads to⁶⁷

$$I_p = a\nu^b \quad (1)$$

where a and b are the adjustable parameters, and I_p and ν are the peak current (mA) and scan rate (mV/s), respectively. A b -value of 1 indicates that the current will be controlled by the surface or near-surface redox reactions, and a b -value of 0.5 would indicate semi-infinite linear diffusion-controlled charge transfer kinetics.⁸ The relationship between log(I_p) vs log(ν) reveals the kinetics of charge transfer for all three types of samples, as shown in Figure 6(a) (cathodic peak observed in the 0.4–0.5 V range). The b -values for h-MoO₃ HNs and pure PANI were found to be 0.54 and 1.02, indicating solid-state diffusion and surface-controlled charge transfer kinetics, respectively. However, a mixed behavior was identified for PANI@h-MoO₃ HNs. For scan rates <5 mV/s, PANI@h-MoO₃ follows the characteristics of h-MoO₃ HNs (solid-state diffusion-controlled kinetics), and for scan rates >5 mV/s, the process was controlled by PANI, i.e., surface-controlled kinetics. The scan rate dependent kinetics of the nanocomposites can be explained taking the following assumptions into consideration: (1) at a slow scan rate, electrolyte ions have sufficient time to diffuse through the polyaniline shell⁶⁸ and to reach the surface of h-MoO₃, and (2) due to excessive doping of protons, the state of polyaniline might be affected (changing from emeraldine to fully reduced leucoemeraldine). A similar behavior is also observed by Gohy et al.⁶⁹ in the nanocomposites of LiFePO₄–PTMA. The vertical dotted line in the current-scan rate relationship represents the diffusion-controlled redox kinetics shown by PANI@h-MoO₃ HNs. This highlights the benefit of using a combinatorial approach.

Another feature of PANI@h-MoO₃ HNs is that at scan rates <5 mV/s the shifts in peak voltage (observed in 0.4–0.5 V range) are small (<30 mV) when compared to the pristine h-MoO₃ HNs (~80 mV peak shift), as shown in Figure 6(b). This indicates that the presence of a PANI shell over the h-MoO₃ core effectively circumvents the abuse of voltage, which is prone at slow scan rates. The absence of a tail in CV curves (Figure 5(a)) for PANI@h-MoO₃ is indicating this behavior. The large shifts in peak voltage (>100 mV) at slow scan rates is mainly associated with the phase change of the materials during the faradic process as identified in many Li-ion intercalation materials such as LiCoO₂.⁷⁰ Therefore, it is conclusive that the presence of a PANI shell over the h-MoO₃ core not only improves the electrochemical performance of h-MoO₃ in terms of specific capacitance and cycling stability but also effectively extends the potential window (lack of tail in CV curves, Figure 5(a)). Attributed to the dual charge transfer kinetics associated with PANI and h-MoO₃ (<5 mV/s—diffusion controlled, >5 mV/s—surface controlled), an improved electrochemical performance of PANI@h-MoO₃ HNs was realized. The contributions of surface-controlled kinetics and diffusion-controlled kinetics to the overall performance were determined to be ~64%, 36% and ~38%, 62% in PANI@h-MoO₃ HNs and h-MoO₃ HNs, respectively (using an approach originally

introduced by Trasatti et al.¹⁰ and recently used by Lee et al.⁷¹ and Dunn et al.,¹² Supporting Information, Figure S11) as represented in Figure 6(c). From Figure 6(c), it is evident that the presence of PANI over the surface of h-MoO₃ solely contributes to the surface redox reactions.

In this work, we combined h-MoO₃ HNs and PANI to form a new pseudocapacitive electrode material. In h-MoO₃, charges are mainly stored through diffusion-controlled redox reactions, while surface-controlled redox reactions are responsible for the charge storage in PANI. Attributed to the coexistence of dual charge-storage kinetics in PANI@h-MoO₃ HNs, an improved specific capacitance is obtained. The combination approach, i.e., PANI@h-MoO₃ HNs, offers several other benefits, such as improved rate capability due to conducting PANI shell and improved cycling life due to hollow nanorod structure of h-MoO₃. Although the specific capacitance value obtained here is less than or comparable to that of carbonaceous materials/polyaniline (a comparison table is presented in Supporting Information, Table S1), this material system offers insights and illustrates the synergistic dual charge-storage kinetics, besides improved cycling life.

We have explicitly shown that the integration of the surface-controlled active (PANI) component with the diffusion-controlled active (h-MoO₃) component leads to a hybrid material, which possesses characteristics of both the constituents.

4. CONCLUSIONS

This study illustrates the formation of h-MoO₃ hollow nanorods by the cation-exchange-assisted Kirkendall effect and the use of conductive polymer shell to realize improved electrochemical performance of h-MoO₃. The combination of redox-active materials (PANI@h-MoO₃ HNs) reinforced the pseudocapacitive performance of the nanocomposites at all applied currents, when compared with PANI or pristine h-MoO₃ HNs. The presence of a PANI shell over the h-MoO₃ core significantly improves the cycling stability of the nanocomposites. The surface-controlled and diffusion-controlled charge transfer kinetics can be delineated. This work contributes significantly not only to the advancement of the synthetic approach to make a nanocomposite of redox active materials but also to the fundamental understanding on improving electrochemical performance of the hybrid nanocomposites.

■ ASSOCIATED CONTENT

Supporting Information

DSC and XRD analysis of h-MoO₃ before and after annealing, FESEM micrographs of h-MoO₃ nanorods and pure PANI powder, TEM micrographs of PANI@h-MoO₃ prepared at various oxidant to aniline molar ratios, IR spectra of PANI@h-MoO₃ prepared using various oxidant to aniline molar ratios, TGA profiles of the as-prepared h-MoO₃ HNs, PANI, and PANI@h-MoO₃ HNs, cyclic voltammograms (CVs) of h-MoO₃ nanorods and h-MoO₃ hollow nanorods, CVs of the as-prepared electrodes at various scan rates, CVs of the samples prepared using higher molar ratios of oxidant to aniline, charge\discharge profiles of all three types of samples at various current densities, charge\discharge profiles of the samples prepared using higher molar ratios of oxidant to aniline, determination of the capacitive-controlled and diffusion-controlled contributions, and performance comparison table.

This material is available free of charge via the Internet at <http://pubs.acs.org>.

AUTHOR INFORMATION

Corresponding Author

*E-mail: pslee@nut.edu.sg.

Notes

The authors declare no competing financial interest.

ACKNOWLEDGMENTS

Vipin Kumar acknowledges the research scholarship provided by Nanyang Technological University in Singapore. This work is supported by Temasek Laboratories @ NTU Singapore under project no. TLSP13-02.

REFERENCES

- (1) Zhao, X.; Sánchez, B. M.; Dobson, P. J.; Grant, P. S. The Role of Nanomaterials in Redox-Based Supercapacitors for next Generation Energy Storage Devices. *Nanoscale* **2011**, *3*, 839–855.
- (2) Lokhande, C. D.; Dubal, D. P.; Joo, O. S. Metal Oxide Thin Film Based Supercapacitors. *Curr. Appl. Phys.* **2011**, *11*, 255–270.
- (3) Jayalakshmi, M.; Balasubramanian, K. Simple Capacitors to Supercapacitors—An Overview. *Int. J. Electrochem. Soc.* **2008**, *3*, 1196–1217.
- (4) Lu, P.; Xue, D.; Yang, H.; Liu, Y. Supercapacitor and Nanoscale research towards electrochemical energy storage. *Int. J. Smart Nano Mater.* **2013**, *4*, 2–26.
- (5) Sumboja, A.; Foo, C. Y.; Yan, J.; Yan, C.; Gupta, R. K.; Lee, P. S. Significant Electrochemical Stability of Manganese Dioxide/polyaniline Coaxial Nanowires by Self-Terminated Double Surfactant Polymerization for Pseudocapacitor Electrode. *J. Mater. Chem.* **2012**, *22*, 23921.
- (6) Weng, T. C.; Teng, H. Characterization of High Porosity Carbon Electrodes Derived from Mesophase Pitch for Electric Double-Layer Capacitors. *J. Electrochem. Soc.* **2001**, *148*, A368.
- (7) Brezesinski, T.; Wang, J.; Tolbert, S. H.; Dunn, B. Ordered Mesoporous Alpha-MoO₃ with Iso-Oriented Nanocrystalline Walls for Thin-Film Pseudocapacitors. *Nat. Mater.* **2010**, *9*, 146–151.
- (8) Augustyn, V.; Come, J.; Lowe, M. A.; Kim, J. W.; Taberna, P. L.; Tolbert, S. H.; Abruña, H. D.; Simon, P.; Dunn, B. High-Rate Electrochemical Energy Storage through Li⁺ Intercalation Pseudocapacitance. *Nat. Mater.* **2013**, *12*, 518–522.
- (9) Yu, Z.; Duong, B.; Abbott, D.; Thomas, J. Highly Ordered MnO₂ Nanopillars for Enhanced Supercapacitor Performance. *Adv. Mater.* **2013**, *25*, 3302–3306.
- (10) Aridzone, S.; Fregonara, G.; Trasatti, S. "Inner" and "Outer" Active Surface of RuO₂ Electrodes. *Electrochim. Acta* **1990**, *35*, 263–267.
- (11) Jirkovský, J.; Makarova, M.; Krtík, P. The Effect of Coherent Domain Size on the Insertion Activity of Nanocrystalline RuO₂. *J. Electrochem. Soc.* **2005**, *152*, A1613–A1619.
- (12) Kim, J. W.; Augustyn, V.; Dunn, B. The Effect of Crystallinity on the Rapid Pseudocapacitive Response of Nb₂O₅. *Adv. Energy Mater.* **2012**, *2*, 141–148.
- (13) Lou, X. W.; Zeng, H. C. Hydrothermal Synthesis of α-MoO₃ Nanorods via Acidification of Ammonium Heptamolybdate Tetrahydrate. *Chem. Mater.* **2002**, *14*, 4781–4789.
- (14) Yao, D. D.; Ou, J. Z.; Latham, K.; Zhuiykov, S.; O'Mullane, A. P.; Kalantar-zadeh, K. Electrodeposited α- and β-Phase MoO₃ Films and Investigation of their gasochromic properties. *Cryst. Growth Des.* **2012**, *12*, 1865–1870.
- (15) Seguin, L.; Figlarz, M.; Cavagnat, R.; Lassegues, J. C. Infrared and Raman Spectra of MoO₃ Molybdenum Trioxides and MoO₃·xH₂O Molybdenum Trioxide Hydrates. *Spectrochim. Acta, Part A* **1995**, *51*, 1323–1344.
- (16) Murugan, R.; Ghule, A.; Bhongale, C.; Chang, H. Thermo-Raman Investigations on Structural Transformations in Hydrated MoO₃. *J. Mater. Chem.* **2000**, *10*, 2157–2162.
- (17) Alsaif, M. M. Y. A.; Latham, K.; Field, M. R.; Yao, D. D.; Medhekar, N. V.; Medhekar, N. V.; Beane, G. A.; Kaner, R. B.; Russo, S. P.; Ou, J. Z.; et al. Tunable Plasmon Resonances in Two-Dimensional Molybdenum Oxide Nanoflakes. *Adv. Mater.* **2014**, *26*, 3931–3937.
- (18) Hamwi, S.; Meyer, J.; Winkler, T.; Riedl, T.; Kowalsky, W. P-Type Doping Efficiency of MoO₃ in Organic Hole Transport Materials. *Appl. Phys. Lett.* **2009**, *94*, 253307.
- (19) Chen, D.; Liu, M.; Yin, L.; Li, T.; Yang, Z.; Li, X.; Fan, B.; Wang, H.; Zhang, R.; Li, Z.; et al. Single-Crystalline MoO₃ Nanoplates: Topochemical Synthesis and Enhanced Ethanol-Sensing Performance. *J. Mater. Chem.* **2011**, *21*, 9332.
- (20) Balendhran, S.; Walia, S.; Alsaif, M.; Nguyen, E. P.; Zhen, J.; Zhuiykov, S.; Sriram, S.; Bhaskaran, M.; Kalantar-zadeh, K. Field Effect Biosensing Platform Based on 2D α-MoO₃. *ACS Nano* **2013**, *11*, 9753–9760.
- (21) Rahmani, M. B.; Keshmiri, S. H.; Yu, J.; Sadek, A. Z.; Al-Mashat, L.; Moafi, A.; Latham, K.; Li, Y. X.; Włodarski, W.; Kalantar-zadeh, K. Gas Sensing Properties of Thermally Evaporated Lamellar MoO₃. *Sens. Actuator, B-Chem.* **2010**, *145*, 13–19.
- (22) Chen, Y. J.; Gao, X. M.; Di, X. P.; Ouyang, Q. Y.; Gao, P.; Qi, L. H.; Li, C.-Y.; Zhu, C. L. Porous Iron Molybdate Nanorods: In Situ Diffusion Synthesis and Low-Temperature H₂S Gas Sensing. *ACS Appl. Mater. Interfaces* **2013**, *5*, 3267–3274.
- (23) Wang, J.; Rose, K. C.; Lieber, C. M. Load-Independent Friction: MoO₃ Nanocrystal Lubricants. *J. Phys. Chem. B* **1999**, *103*, 0–4.
- (24) Tao, T.; Glushenkov, A. M.; Zhang, C.; Zhang, H.; Zhou, D.; Guo, Z.; Liu, H. K.; Chen, Q.; Hu, H.; Chen, Y. MoO₃ Nanoparticles Dispersed Uniformly in Carbon Matrix: A High Capacity Composite Anode for Li-Ion Batteries. *J. Mater. Chem.* **2011**, *21*, 9350.
- (25) Mai, L. Q.; Hu, B.; Chen, W.; Qi, Y. Y.; Lao, C. S.; Yang, R. S.; Dai, Y.; Wang, Z. L. Lithiated MoO₃ Nanobelts with Greatly Improved Performance for Lithium Batteries. *Adv. Mater.* **2007**, *19*, 3712–3716.
- (26) Chernova, N. A.; Roppolo, M.; Dillon, A. C.; Whittingham, M. S. Layered Vanadium and Molybdenum Oxides: Batteries and Electrochromics. *J. Mater. Chem.* **2009**, *19*, 2526.
- (27) Sugimoto, W.; Ohnuma, T.; Murakami, Y.; Takasu, Y. Molybdenum Oxide/Carbon Composite Electrodes as Electrochemical Supercapacitors. *Electrochim. Solid State Lett.* **2001**, *4*, A145.
- (28) Mahmood, Q.; Kim, W. S.; Park, H. S. Structure and Compositional Control of MoO₃ Hybrids Assembled by Nanoribbons for Improved Pseudocapacitor Rate and Cycle Performance. *Nanoscale* **2012**, *4*, 7855–7860.
- (29) Mai, L.; Hu, B.; Qi, Y.; Dai, Y.; Chen, W. Improved Cycling Performance of Directly Lithiated MoO₃ Nanobelts. *Int. J. Electrochem. Sci.* **2008**, *3*, 216–222.
- (30) Tang, Q.; Wang, L.; Zhu, K.; Shan, Z.; Qin, X. Synthesis and Electrochemical Properties of H-MoO₃/graphene Composite. *Mater. Lett.* **2013**, *100*, 127–129.
- (31) Jiang, F.; Li, W.; Zou, R.; Liu, Q.; Xu, K.; An, L.; Hu, J. MoO₃/PANI Coaxial Heterostructure Nanobelts by In Situ Polymerization for High Performance Supercapacitors. *Nano Energy* **2014**, *7*, 72–79.
- (32) Liu, Y.; Zhang, B.; Yang, Y.; Chang, Z.; Wen, Z.; Wu, Y. Polypyrrole-Coated α-MoO₃ Nanobelts with Good Electrochemical Performance as Anode Materials for Aqueous Supercapacitors. *J. Mater. Chem. A* **2013**, *1*, 13582.
- (33) Zhang, X.; Zeng, X.; Yang, M.; Qi, Y. Investigation of a Branchlike MoO₃/polypyrrole Hybrid with Enhanced Electrochemical Performance Used as an Electrode in Supercapacitors. *ACS Appl. Mater. Interfaces* **2014**, *6*.
- (34) Fan, H. J.; Gösele, U.; Zacharias, M. Formation of Nanotubes and Hollow Nanoparticles Based on Kirkendall and Diffusion Processes: A Review. *Small* **2007**, *3*, 1660–1671.
- (35) Oh, M. H.; Yu, T.; Yu, S. H.; Lim, B.; Ko, K. T.; Willinger, M. G.; Seo, D. H.; Kim, B. H.; Cho, M. G.; Park, J. H.; et al. Galvanic

- Replacement Reactions in Metal Oxide Nanocrystals. *Science* **2013**, *340*, 964–968.
- (36) Wang, W.; Dhal, M.; Yin, Y. Hollow Nanocrystals through the Nanoscale Kirkendall Effect. *Chem. Mater.* **2013**, *25*, 89–96.
- (37) Chun Zeng, H. Ostwald Ripening: A Synthetic Approach for Hollow Nanomaterials. *Curr. Nanosci.* **2007**, *3*, 117.
- (38) Lei, Z.; Chen, Z.; Zhao, X. S. Growth of Polyaniline on Hollow Carbon Spheres for Enhancing Electrocapacitance. *J. Phys. Chem. C* **2010**, *114*, 19867–19874.
- (39) Lai, X.; Halpert, J. E.; Wang, D. Recent Advances in Micro-/nano-Structured Hollow Spheres for Energy Applications: From Simple to Complex Systems. *Energy Environ. Sci.* **2012**, *5*, 5604.
- (40) Fan, S. Q.; Fang, B.; Kim, J. H.; Kim, J.-J.; Yu, J.-S.; Ko, J. Hierarchical Nanostructured Spherical Carbon with Hollow Core/mesoporous Shell as a Highly Efficient Counter Electrode in CdSe Quantum-Dot-Sensitized Solar Cells. *Appl. Phys. Lett.* **2010**, *96*, 063501.
- (41) Wen, Z.; Wang, Q.; Zhang, Q.; Li, J. Hollow Carbon Spheres with Wide Size Distribution as Anode Catalyst Support for Direct Methanol Fuel Cells. *Electrochem. Commun.* **2007**, *9*, 1867–1872.
- (42) Lin, M. F.; Thakur, V. K.; Tan, E. J.; Lee, P. S. Dopant Induced Hollow BaTiO₃ Nanostructures for Application in High Performance Capacitors. *J. Mater. Chem.* **2011**, *21*, 16500.
- (43) Guo, P.; Song, H.; Chen, X. Hollow Graphene Oxide Spheres Self-Assembled by W/O Emulsion. *J. Mater. Chem.* **2010**, *20*, 4867.
- (44) Cao, C. Y.; Guo, W.; Cui, Z.-M.; Song, W.-G.; Cai, W. Microwave-Assisted Gas/liquid Interfacial Synthesis of Flowerlike NiO Hollow Nanosphere Precursors and Their Application as Supercapacitor Electrodes. *J. Mater. Chem.* **2011**, *21*, 3204.
- (45) Chen, H.; Zhou, S.; Chen, M.; Wu, L. Reduced Graphene Oxide-MnO₂ Hollow Sphere Hybrid Nanostructures as High-Performance Electrochemical Capacitors. *J. Mater. Chem.* **2012**, *22*, 25207.
- (46) Wang, Q.; Jiao, L.; Du, H.; Si, Y.; Wang, Y.; Yuan, H. Co₃S₄ Hollow Nanospheres Grown on Graphene as Advanced Electrode Materials for Supercapacitors. *J. Mater. Chem.* **2012**, *22*, 21387.
- (47) Guan, C.; Xia, X.; Meng, N.; Zeng, Z.; Cao, X.; Soci, C.; Zhang, H.; Fan, H. J. Hollow Core-Shell Nanostructure Supercapacitor Electrodes. *Energy Environ. Sci.* **2012**, 9085–9090.
- (48) Huang, M.; Zhang, Y.; Li, F.; Wang, Z.; Alamus; Hu, N.; Wen, Z.; Liu, Q. Merging of Kirkendall Growth and Ostwald Ripening: CuO@MnO₂ Core-Shell Architectures for Asymmetric Supercapacitors. *Sci. Rep.* **2014**, *4*, 4518.
- (49) Kumar, V.; Wang, X.; Lee, P. S. Synthesis of Pyramidal and Prismatic Hexagonal MoO₃ Nanorods Using Thiourea. *CrystEngComm* **2013**, *15*, 7663.
- (50) Wang, L.; Peng, B.; Guo, X.; Ding, W.; Chen, Y. Ferric Molybdate Nanotubes Synthesized Based on the Kirkendall Effect and Their Catalytic Property for Propene Epoxidation by Air. *Chem. Commun.* **2009**, 1565–1567.
- (51) Chaudhari, H. K.; Kelkar, D. S. X-ray Diffraction Study of Doped Polyaniline. *J. Appl. Polym. Sci.* **1996**, *62*, 15–18.
- (52) Abdiryim, T.; Jamal, R.; Nurulla, I. Doping Effect of Organic Sulphonic Acids on the Solid-State Synthesized Polyaniline. *J. Appl. Polym. Sci.* **2007**, *105*, 576.
- (53) Lunk, H. J.; Hartl, H.; Hartl, M. A.; Fait, M. J. G.; Shenderovich, I. G.; Feist, M.; Frisk, T. A.; Daemen, L. L.; Mauder, D.; Eckelt, R.; et al. Hexagonal Molybdenum Trioxide Known for 100 Years and Still a Fount of New Discoveries. *Inorg. Chem.* **2010**, *49*, 9400–9408.
- (54) Zheng, L.; Xu, Y.; Jin, D.; Xie, Y. Novel Metastable Hexagonal MoO₃ Nanobelts: Synthesis, Photochromic, and Electrochromic Properties. *Chem. Mater.* **2009**, *21*, 5681–5690.
- (55) Kumar, V.; Sumboja, A.; Wang, J.; Bhavanasi, V.; Nguyen, V. C.; Lee, P. S. Topotactic Phase Transformation of Hexagonal MoO₃ to Layered MoO₃-II and Its Two-Dimensional (2D) Nanosheets. *Chem. Mater.* **2014**, *26*, 5533–5539.
- (56) Zhang, Z.; Wei, Z.; Wan, M. Nanostructures of Polyaniline Doped with Inorganic Acids. *Macromolecules* **2002**, *35*, 5937–5942.
- (57) Pan, L. J.; Pu, L.; Shi, Y.; Song, S. Y.; Xu, Z.; Zhang, R.; Zheng, Y. D. Synthesis of Polyaniline Nanotubes with a Reactive Template of Manganese Oxide. *Adv. Mater.* **2007**, *19*, 461–464.
- (58) Sapurina, I. Y.; Shishov, M. A. *Oxidative Polymerization of Aniline: Molecular Synthesis of Polyaniline and the Formation of Supramolecular Structures*; InTech: Winchester, U. K., 2012.
- (59) Nestorovic, G.; Jeremic, K.; Jovanovic, S. Kinetics of Aniline Polymerization Initiated with iron(III) Chloride. *J. Serb. Chem. Soc.* **2006**, *71*, 895–904.
- (60) Rivest, J. B.; Jain, P. K. Cation Exchange on the Nanoscale: An Emerging Technique for New Material Synthesis, Device Fabrication, and Chemical Sensing. *Chem. Soc. Rev.* **2013**, *42*, 89–96.
- (61) Son, D. H.; Hughes, S. M.; Yin, Y.; Paul Alivisatos, A. Cation Exchange Reactions in Ionic Nanocrystals. *Science* **2004**, *306*, 1009–1012.
- (62) Xia, X.; Hao, Q.; Lei, W.; Wang, W.; Wang, H.; Wang, X. Reduced-Graphene Oxide/molybdenum Oxide/polyaniline Ternary Composite for High Energy Density Supercapacitors: Synthesis and Properties. *J. Mater. Chem.* **2012**, *22*, 8314.
- (63) Zheng, L.; Xu, Y.; Jin, D.; Xie, Y. Polyaniline-Intercalated Molybdenum Oxide Nanocomposites: Simultaneous Synthesis and Their Enhanced Application for Supercapacitor. *Chem. Asian J.* **2011**, *6*, 1505–1514.
- (64) Zhou, X.; Ma, L.; Xu, X.; Feng, Z. Thermal decomposition synthesis of MoO₃ for application in electrochemical supercapacitors. *Adv. Mater. Res.* **2014**, *1008*, 361–364.
- (65) Hsieh, C. T.; Lin, C. Y.; Chen, Y. F.; Lin, J. S.; Teng, H. Silver Nanorods Attached to Graphene Sheets as Anode Materials for Lithium-Ion Batteries. *Carbon* **2013**, *62*, 109–116.
- (66) Yang, Q.; Lu, Z.; Liu, J.; Lei, X.; Chang, Z.; Luo, L.; Sun, X. Metal Oxide and Hydroxide Nanoarrays: Hydrothermal Synthesis and Applications as Supercapacitors and Nanocatalysts. *Prog. Nat. Sci.: Mater. Int.* **2013**, *23*, 351–366.
- (67) Lindstro, H.; So, S.; Solbrand, A.; Hjelm, J.; Hagfeldt, A.; Lindquist, S. Li⁺ Ion Insertion in TiO₂ (Anatase). 2. Voltammetry on Nanoporous Films. *J. Phys. Chem. B* **1997**, *101*, 7717–7722.
- (68) Jafeen, M. J. M.; Careem, M. a.; Skaarup, S. A Novel Method for the Determination of Membrane Hydration Numbers of Cations in Conducting Polymers. *J. Solid State Electrochem.* **2011**, *16*, 1753–1759.
- (69) Vald, A.; Singh, N.; Rolland, J.; Melinete, S.; Ajayan, p. M.; Gohy, J. F. Hybrid Supercapacitor-Battery Materials For Fast Electrochemical Charge Storge. *Sci. Rep.* **2014**, *4*, 4315.
- (70) Xia, H.; Lu, L.; Ceder, G. Substrate Effect on the Microstructure and Electrochemical Properties of LiCoO₂ Thin Films Grown by PLD. *J. Alloy. Compd.* **2006**, *417*, 304–310.
- (71) Wang, X.; Liu, W. S.; Lu, X.; Lee, P. S. Dodecyl Sulfate-Induced Fast Faradic Process in Nickel Cobalt Oxide-reduced Graphite Oxide Composite Material and Its Application for Asymmetric Supercapacitor Device. *J. Mater. Chem.* **2012**, *22*, 23114.